Shape optimisation of an oscillating body in fluid flow by adjoint equation and ALE finite element methods

Article *in* International Journal of Computational Fluid Dynamics · May 2008

DOI: 10.1080/10618560801914447

CITATIONS
8

READS
29

2 authors, including:

Mutsuto Kawahara
Chuo University
303 PUBLICATIONS **2,842** CITATIONS

SEE PROFILE

Shape Optimization of an Oscillating Body in Fluid Flow by Adjoint Equation and ALE Finite Element Methods

Hiroki YOSHIDA * and Mutsuto KAWAHARA †

Abstract

The purpose of this study is to determine the minimum drag and lift shape of an oscillating body located in the transient incompressible viscous fluid flow by the Arbitrary Lagrangian Eulerian finite element method and an optimal control theory in which a performance function is expressed by the drag and lift forces. The performance function should be minimized satisfying the state equation and constant volume condition. This problem can be transformed into the minimization problem without constraint condition by the Lagrange multiplier method. The adjoint equation and gradient are used to the renewal of shape of the body. In this study, as a minimization technique, the weighted gradient method is applied. The final shape is obtained of which drag and lift forces are reduced by 66.2 % and 92.8 %, respectively. The final shape obtained by this study is compared with the final shape of the non-oscillating body. The final shape of the oscillating body is obtained which is significantly different from the non-oscillating body.

1 INTRODUCTION

The shape determination of a body minimizing fluid force is one of the main subject of the fluid dynamics. Until recent years, shape optimization of a body located in a fluid flow has been generally carried out assuming the body does not move by the fluid flow [1)−10)]. Pironneau [1),2)] proposed the algorithm of shape optimization, which is to change shape of a body optimally using the gradient of the variation with respect to coordinates by semi-analytical forms.

On the optimal control theory, control value which makes phenomenon an optimal state can be obtained. To determine the optimal state, the performance function is introduced, which consists of the fluid force acting on the target body. The fluid force is divided into the drag and lift forces, which are obtained by the state equation. The performance function should be minimized satisfying the state equation. Therefore, this optimal control problem results in the minimization problem with constraint conditions. Those researches have presented by Kawahara et al. [4),7),9)] and many other researchers. Ogawa and Kawahara [7)] presented the drag force minimization problem located in the low Reynolds number flow without considering the oscillation of the body. Yagi and Kawahara [9),10)] also presented the drag force minimization problem located in the incompressible Navier-Stokes flow without considering the oscillation of the body. The gradient used to the renewal shape is obtained by the formulation of optimal control. Conventionally, the formulation is performed after giving the finite element approximation for the state equation. Then, the gradient becomes the direct function of coordinates treated as design variable, which is called as the sensitivity method.

In the present study, the optimal shape determination problem of the minimum drag and lift forces subjected to the oscillating body is carried out. Considering that the volume of a body should be kept constant, the volume constraint is introduced. If the performance function is minimized, the state is optimized. The control value which is a coordinate of the body, can be obtained. In addition, to consider an oscillation of body, this problem is treated as a fluid-structure interaction problem. The Arbitrary Lagrangian Eulerian method is effectively introduced to solve moving boundary problem [14),15)].

The feature of this study is to consider an oscillation of a body, because a body located in the fluid

*Department of civil Engineering, Chuo University Kasuga 1-13-27, Bunkyo-ku, Tokyo, JAPAN
†Department of civil Engineering, Chuo University Kasuga 1-13-27, Bunkyo-ku, Tokyo, JAPAN
E-mail : kawa@civil.chuo-u.ac.jp

flow is actually forced by the flow and the minute vibration is occurred. The computation of the motion of body and the gradient for the renewal of shape is precisely described. The Reynolds number is set as $Re = 250$. The drag and lift forces are compared between of initial and final shapes of the body. The peak value of the lift force is reduced by 93 %. A shape variation of the body at initial and final stages through iteration procedure is obtained. The final shape of the oscillating body is more symmetrical than that of the non-oscillating body. The peak value of the lift force of the oscillating body is as much as twice of the non-oscillating body.

2 GOVERNING EQUATION

2.1 ALE Description

Indicial notation and summation convention with repeated indices are used in this paper. Description of a motion of a body is expressed by the Lagrangian, Eulerian and reference coordinate systems, X_i, x_i and χ_i, respectively. An arbitrary coordinate system χ_i that is independent of the first two is introduced and is called as the reference coordinate system. Relation between the real time derivative and the reference time derivative is as follows:

$$\frac{dx_i(\chi_i,t)}{dt} = \frac{\partial x_i(\chi_i,t)}{\partial t} + \frac{\partial x_i(\chi_i,t)}{\partial \chi_j} \cdot \frac{\partial \chi_j(X_i,t)}{\partial t}\Big|_{X_i}. \tag{1}$$

Putting

$$\omega_j = \frac{\partial \chi_j(X_i,t)}{\partial t}, \tag{2}$$

eq.(1) can be written in the following form.

$$\frac{\partial x_i(X_i,t)}{\partial t}\Big|_{X_i} = \frac{\partial x_i(\chi_i,t)}{\partial t}\Big|_{\chi_i} + \frac{\partial x_i(\chi_i,t)}{\partial \chi_j} \cdot \frac{\partial \chi_j}{\partial t} \tag{3}$$

$$= \frac{\partial x_i(\chi_i,t)}{\partial t}\Big|_{\chi_i} + \omega_j \cdot \frac{\partial x_i}{\partial \chi_j} \tag{4}$$

Introducing b_i of the material point for the reference coordinate system

$$b_i = u_i - \hat{u}_i = \omega_j \cdot \frac{\partial x_i}{\partial \chi_j}, \tag{5}$$

where

$$u_i = \frac{\partial x_i(X_i,t)}{\partial t}\Big|_{X_i}, \tag{6}$$

$$\hat{u}_i = \frac{\partial x_i(\chi_i,t)}{\partial t}\Big|_{\chi_i}. \tag{7}$$

Substituting the velocity relation equation (5) into the reference time derivative equation, the function of reference time derivative in Euler form is obtained.

$$\frac{\partial u_i(X_i,t)}{\partial t}\Big|_{X_i} = \frac{\partial u_i(x_i(\chi_i,t),t)}{\partial t}\Big|_{\chi_i} + b_j \cdot \frac{\partial u_i(x_i(\chi_i,t),t)}{\partial x_j(\chi_i,t)}. \tag{8}$$

This is the basic equation of the time derivative in the ALE method.

2.2 Navier-Stokes equation described by ALE description

Let Ω denote the computational domain with boundary Γ, and suppose that an incompressible transient viscous flow occupies Ω. The Navier-Stokes equation can be expressed by the non-dimensional form as follows:

$$\dot{u}_i + b_j u_{i,j} + p_{,i} - \nu(u_{i,j} + u_{j,i})_{,j} = 0 \quad \text{in} \quad \Omega, \tag{9}$$

$$u_{i,i} = 0 \quad \text{in} \quad \Omega, \tag{10}$$

where u_i, p and ν are velocity defined in eq.(6), pressure and kinematic viscosity coefficient, respectively, in which ν is the inverse of Reynolds number. The relative velocity of material point using the reference coordinate system is denoted by b_i.

Consider a typical problem described in Fig.1, in which a solid body B with the boundary Γ_B is laid in an external flow. The boundary conditions are given in eqs.(11) - (14) in which eqs.(13) and (14) mean the slip and non-slip conditions on the boundaries. The initial condition is in eq.(15).

$$u_i = (U, 0) \quad \text{on} \quad \Gamma_U, \tag{11}$$

$$t_i = 0 \quad \text{on} \quad \Gamma_D, \tag{12}$$

$$t_1 = 0, \quad u_2 = 0 \quad \text{on} \quad \Gamma_S, \tag{13}$$

$$u_i = 0 \quad \text{on} \quad \Gamma_B, \tag{14}$$

$$u_i(t_0) = \hat{u}_{i0} \quad \text{in} \quad \Omega, \tag{15}$$

where

$$t_i = \{-p\delta_{ij} + \nu(u_{i,j} + u_{j,i})\}n_j, \tag{16}$$

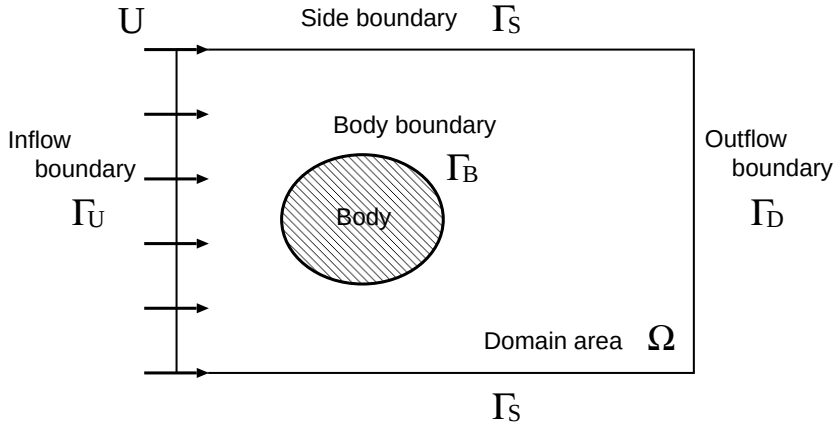

Fig.1 Computational domain and boundary condition

in which t_i is the traction and n_j is unit outward normal to the boundary Γ, respectively. The fluid force acting on the body B is defined by F_i, where F_1 and F_2 are drag and lift forces respectively. The fluid force F_i is obtained by integrating the traction t_i on the boundary Γ_B as follows:

$$F_i = -\int_{\Gamma_B} t_i d\Gamma. \tag{17}$$

2.3 Body movement

A rigid body is assumed to have three-degree-of-freedom, of which components are displacement X_i and rotation θ, where X_i means x, y displacements. The equation of motion is expressed as follows:

$$m\ddot{X}_i + c\dot{X}_i + kX_i = F_i, \tag{18}$$

$$I\ddot{\theta} + c_\theta\dot{\theta} + k_\theta\theta = M, \tag{19}$$

$$F_i = \left\{ \sum_{j=1}^{n} f_{xj}, \quad \sum_{j=1}^{n} f_{yj} \right\} = -\int_{\Gamma_B} t_i d\Gamma, \tag{20}$$

$$M = \sum_{j=1}^{n} (y_j \cdot f_{xj} - x_j \cdot f_{yj}), \tag{21}$$

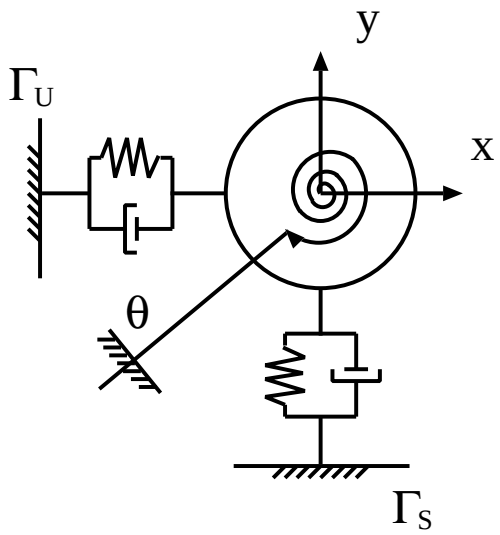

Fig.2 Model

where m, c and k are mass, damping and elastic coefficients and I and M are the inertial moment and moment force, respectively.

3 FORMULATION OF OPTIMAL SHAPE

The optimal shape is pursued to minimize the square sum of the fluid force subjected to the body located in the fluid flow. The optimization method is based on the adjoint equation method in the optimal control theory. Computing the adjoint equation, the gradient of the performance function with respect to the surface coordinate of the body can be described by the adjoint variable. Based on the bubble function finite element method the weighed gradient method is efficiently utilized.

3.1 Performance function

The performance function J is defined to find the surface coordinates of target body so as to minimize the fluid force. It is defined by the square sum of the fluid force expressed as follows:

$$J = \frac{1}{2}\int_{t_0}^{t_f}(q_1 F_1^2 + q_2 F_2^2)dt \tag{22}$$

where q_1 and q_2 are weighting parameters. On the optimal control theory, considering that the performance function defined is minimized, the optimal condition can be derived.

3.2 Volume constant condition

The shape of a body should be optimized keeping the volume constant at each iteration cycle. To keep the volume of a body means to keep the volume of whole computational domain. The volume constraint condition yields as follows:

$$\sum_{e=1}^{m}\{a_e(X_i)\}^{(l)} - A_0 = 0 \qquad \text{in } \Omega, \tag{23}$$

where $a_e(X_i)$ is the volume of each element, m is the total number of element inside the body, and A_0 is the volume of the initial state, respectively.

3.3 Extended performance function

The performance function should be minimized satisfying the constraint conditions which are the state equations (9) and (10) and the volume constant condition (23). The Lagrange multiplier method is suitable for minimization problems with the constraint conditions. This problem can be transformed into the minimization problem without constraint conditions. The Lagrange multipliers for the state equations (9) and (10) and the volume constant condition (23) are defined as the adjoint velocity u_i^*, the adjoint pressure p^* and the adjoint variable λ, respectively. The performance function is extended by adding inner products between the adjoint velocity u_i^*, pressure p^* and the state equations (9) and (10) and between the adjoint variable λ and the volume constant condition (23), respectively. The extended performance function J' is expressed as follows:

$$\begin{aligned} J' &= \frac{1}{2}\int_{t_0}^{t_f}(q_1F_1^2+q_2F_2^2)dt \\ &- \int_{t_0}^{t_f}\int_{\Omega} u_i^*\{\dot{u}_i+b_ju_{i,j}+p_{,i}-\nu(u_{i,j}+u_{j,i})_{,j}\}d\Omega dt \\ &+ \int_{t_0}^{t_f}\int_{\Omega} p^*u_{i,i}d\Omega dt \\ &+ \lambda[\sum_{e=1}^{m}\{a_e(X_i)\}^{(l)}-A_0]. \end{aligned} \tag{24}$$

3.4 Stationary condition

The minimization problem with constraint conditions results in satisfying the stationary conditions of the extended performance function. The stationary condition can be derived from the first variation of the extended performance function.

$$\begin{aligned} \delta J' = &- \int_{t_0}^{t_f}\int_{\Omega}\delta u_i^*\{\dot{u}_i+b_ju_{i,j}+p_{,i}-\nu(u_{i,j}+u_{j,i})_{,j}\}d\Omega dt \\ &+ \int_{t_0}^{t_f}\int_{\Omega}\delta p^*u_{i,i}d\Omega dt \\ &- \int_{t_0}^{t_f}\int_{\Omega}\{-\dot{u}_i^*-(b_ju_i^*)_{,j}+p_{,i}^*-\nu(u_{i,j}^*+u_{j,i}^*)_{,j}\}\delta u_i d\Omega dt \\ &+ \int_{t_0}^{t_f}\int_{\Omega}u_{i,i}^*\delta p d\Omega dt \\ &+ \int_{t_0}^{t_f}\int_{\Gamma_U}u_i^*\delta t_i d\Gamma dt+\int_{t_0}^{t_f}\int_{\Gamma_S}u_2^*\delta t_2 d\Gamma dt \\ &- \int_{t_0}^{t_f}\int_{\Gamma_D}s_i\delta u_i d\Gamma dt-\int_{t_0}^{t_f}\int_{\Gamma_S}s_1\delta u_1 d\Gamma dt-\int_{t_0}^{t_f}\int_{\Gamma_B}s_i\delta u_i d\Gamma dt \\ &+ \int_{t_0}^{t_f}\int_{\Gamma_B}(u_1^*-q_1F_1)\delta t_1 d\Gamma dt+\int_{t_0}^{t_f}\int_{\Gamma_B}(u_2^*-q_2F_2)\delta t_2 d\Gamma dt \\ &- \int_{\Omega}u_i(t_f)^*\delta u_i(t_f)d\Omega+\int_{\Omega}u_i(t_0)^*\delta u_i(t_0)d\Omega, \end{aligned} \tag{25}$$

where

$$s_i = \{b_ju_i^*-p^*\delta_{ij}+\nu(u_{i,j}^*+u_{j,i}^*)\}n_j. \tag{26}$$

The stationary condition means that the first variation of the extended performance function vanishes.

$$\delta J' = 0 \tag{27}$$

Considering that each term of eq.(25) equals zero, the stationary conditions are obtained as follows:

$$
\begin{aligned}
-\dot{u}_i^* - (b_j u_i^*)_{,j} + p_{,i}^* - \nu(u_{i,j}^* + u_{j,i}^*)_{,j} &= 0 \qquad \text{in } \Omega, && (28)\\
u_{i,i}^* &= 0 \qquad \text{in } \Omega, && (29)\\
u_i^* &= 0 \qquad \text{on } \Gamma_U, && (30)\\
s_i &= 0 \qquad \text{on } \Gamma_D, && (31)\\
s_1 = 0, \quad u_2^* &= 0 \qquad \text{on } \Gamma_S, && (32)\\
u_1^* - q_1 F_1 = 0 \quad u_2^* - q_2 F_2 &= 0 \qquad \text{on } \Gamma_B, && (33)\\
u_{i(t_f)}^* &= 0 \qquad \text{in } \Omega. && (34)
\end{aligned}
$$

Introducing eqs.(28)-(34) into eq.(25) and rearranging, the following equation can be derived.

$$\delta J' = -\int_{t_0}^{t_f} \int_{\Gamma_B} s_i \delta u_i d\Gamma dt \tag{35}$$

The variation δu_i can be expressed by δX_j as:

$$\delta u_i = \frac{\partial u_i}{\partial X_j} \delta X_j = u_{i,j} \delta X_j, \tag{36}$$

where X_j is the coordinate of body which defines the shape of the body. Introducing eq.(36) into eq.(35), it is obtained that

$$\delta J' = -\int_{t_0}^{t_f} \int_{\Gamma_B} s_i u_{i,j} \delta X_j d\Gamma dt. \tag{37}$$

Taking into account that δX_i in eq.(37) is an arbitrary variation, the gradient to adjust the shape of target body, grad(J'), can be expressed as follows:

$$\text{grad}(J') = -s_j u_{j,i}. \tag{38}$$

4 DISCRETIZATION

4.1 Spatial discretization

As the spatial discretization, the finite element method using mixed interpolation presented by Kawahara and his co-workers [4),16)] based on the bubble function is applied to the state and adjoint equations. In this section, only the spatial discretization of velocity and pressure is described for the state equation, because completely the same discretization is applied to the adjoint equation.

The bubble function interpolation for velocity and the linear interpolation for pressure are applied and expressed as follows. For bubble function interpolation:

$$
\begin{aligned}
u_i &= \Phi_1 u_{i1} + \Phi_2 u_{i2} + \Phi_3 u_{i3} + \Phi_4 \tilde{u}_{i4}, && (39)\\
\tilde{u}_{i4} &= u_{i4} - \frac{1}{3}(u_{i1} + u_{i2} + u_{i3}),\\
\Phi_1 = L_1, \quad \Phi_2 = L_2, \quad \Phi_3 &= L_3, \quad \Phi_4 = 27 L_1 L_2 L_3,
\end{aligned}
$$

and for linear interpolation:

$$
\begin{aligned}
p &= \Psi_1 p_1 + \Psi_2 p_2 + \Psi_3 p_3, && (40)\\
\Psi_1 = L_1, \quad \Psi_2 &= L_2, \quad \Psi_3 = L_3,
\end{aligned}
$$

where $\Phi_\alpha(\alpha = 1, 4)$ and $\Psi_\lambda(\lambda = 1, 3)$ are the bubble function interpolation for the velocity as shown in Fig.3 and the linear interpolation for pressure as shown in Fig.4, respectively.

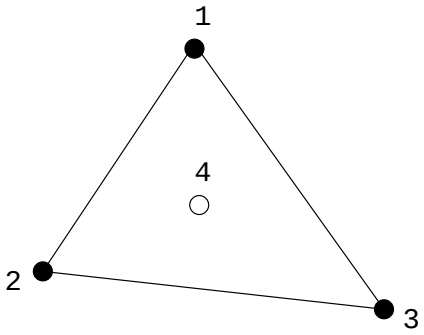

Fig.3 bubble function interpolation

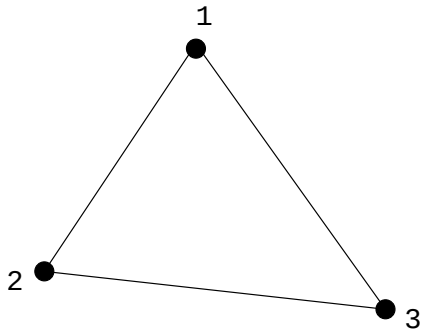

Fig.4 linear interpolation

The numerical viscosity is innovated for the stabilization [13),16)]. The stabilized parameter τ_{eB} which determines the magnitude of the streamline stabilized term. The stabilized parameter τ_{eB} is expressed as follows:

$$\tau_{eB} = \frac{< \phi_e, 1 >^2_{\Omega_e}}{(\nu + \nu')\|\phi_{e,j}\|^2_{\Omega_e} A_e}, \tag{41}$$

where Ω_e is element domain and

$$< u, v >_{\Omega_e} = \int_{\Omega_e} uv d\Omega, \qquad \|u\|^2_{\Omega_e} = \int_{\Omega_e} uu d\Omega, \qquad A_e = \int_{\Omega_e} d\Omega,$$

The integral of bubble function is expressed as follows:

$$< \phi_e, 1 >_{\Omega_e} = \frac{A_e}{3}, \quad \|\phi_{e,j}\|^2_{\Omega_e} = 2A_e g, \quad g = \sum_{i=1}^{2} |\Psi_{\alpha,i}|^2.$$

where ν' is control parameter for the stabilizing action and this value is determined by the fact that τ_{eB} is equal to τ_{eS} and used in the stabilized finite element method as:

$$\tau_{eS} = \left[\left(\frac{2|u_i|}{h_e} \right)^2 + \left(\frac{4\nu}{h_e^2} \right)^2 \right]^{-\frac{1}{2}}, \tag{42}$$

where h_e is an element size.

Generally, the stabilized parameter, expressed in eq.(42), is not equal to the optimal parameter. Thus, the bubble function which gives the optimal viscosity should be introduced. The stabilized operator control parameter is expressed as follows:

$$\frac{< \phi_e, 1 >^2_{\Omega_e}}{(\nu + \nu')\|\phi_{e,j}\|^2_{\Omega_e} A_e} = \tau_{eB}. \tag{43}$$

It is shown that eq.(44) adds stabilized operator control term only at the barycenter point to the equation of motion:

$$\sum_{e=1}^{N_e} \nu' \|\phi_{e,j}\|^2_{\Omega_e} b_e, \tag{44}$$

where N_e and b_e are the total number of elements and barycenter point respectively.

5 WEIGHTED GRADIENT METHOD

As the minimization technique, the weighted gradient method, which seems to be scarcely dependent on the initial value, is applied. In this method, a modified performance function, $K^{(l)}$, which is obtained adding a penalty term to the extended performance function, is introduced. The modified performance function is expressed as follows:

$$K^{(l)} = J'^{(l)} + \frac{1}{2}\Big(X_i^{(l+1)} - X_i^{(l)}\Big)^T W\Big(X_i^{(l+1)} - X_i^{(l)}\Big), \tag{45}$$

where l is iteration number of minimization and W is weighting diagonal matrix, respectively. In case that the modified performance function converges to the minimum, the penalty term can also be zero, i.e., minimization of the modified performance function is equal to the minimization of the extended performance function. Let $X_i^{(l)}$ be the optimal solution, then the following equality holds,

$$\delta K^{(l)} = \mathrm{grad}(J')^{(l)}\delta X_i^{(l)} + W\Big(X_i^{(l+1)} - X_i^{(l)}\Big)\delta X_i^{(l)} \tag{46}$$

From the condition:

$$\delta K^{(l)} = 0. \tag{47}$$

the equation used for the renewal of shape at each iteration cycle is obtained as follows:

$$X_i^{(l+1)} = X_i^{(l)} - \frac{1}{W}\cdot \mathrm{grad}(J')^{(l)}. \tag{48}$$

6 NUMERICAL STUDY

As a numerical study, the fluid force minimization problem of an oscillating body located in the incompressible Navier-Stokes flow by the present method is carried out. Both drag and lift forces are equally used for optimization which means the weighting parameters q_1 and q_2 in eq.(22) are set both 1.0. The Reynolds number is taken as 250. The displacement of the rigid body is limited to vertical direction y. The body shape obtained by the ALE finite element method is compared with the non-oscillating body shape, which is obtained using the same data of the oscillating body for weighting parameters q_1, q_2 and Reynolds number Re.

6.1 Finite element mesh

The computational domain, boundary conditions and the finite element mesh at initial stage are shown in Figs.5 and 6. The body is located in the center of the computational domain. Total numbers of nodes and elements are 2010 and 3812, respectively. In case that the body is located in the left of the computational domain like the Figs.7 and 8, it is known that the difference is caused for the obtained shape. The obtaind shapes which are located in the center and left of domain at $Re = 1.0$ is compared in Fig.9. The obtained shape which is located in the center is symmetric with respect to horizontal and vertical axises, however, the obtained one which is located in the left is symmeric with respect to only horizontal axis. The magnified figure of the initial shape of the body is shown in Fig.10. In this study, the finite element mesh used to determine the shape optimization is composed of the regular mesh in the neighborhood of the body and the irregular delaunay type mesh outside the regular mesh. In case that the irregular mesh in all calculation area is used, the smooth value of the gradient for the renewal of coordinate of shape is not obtained as shown in Fig.11, although the smooth flow is computed. In case that the regular mesh in the neighborhood of the body is utilized, it is possible to get the smooth value of the gradient as shown in Fig.12. In Figs.13 and 14, intermediate configuration of the body and the gradient after 118 iteration cycle are represented. Looking at those figures, it is known that the mesh regularity around the body is important to obtain the stable computation.

6.2 Mesh movement

According to the movement of the rigid body, the finite element mesh should be re-generated. The behavior of an oscillating body is expressed by the motion equations (18) - (21). Because the oscillating body is treated as the rigid body, the deformation is not occurred. The displacement of the vertical direction y is obtained by eq.(18). Changing the boundary configuration, the coordinate of nodes distributed in the whole calculation area can be derived solving the Laplace equation.

$$\nabla \cdot \phi = 0 \qquad \text{in} \quad \Omega \tag{49}$$

$$\phi = 0 \quad \text{on} \quad \Gamma_U, \qquad \phi = 0 \quad \text{on} \quad \Gamma_S, \qquad \phi = 0 \quad \text{on} \quad \Gamma_D, \qquad \phi = y \quad \text{on} \quad \Gamma_B,$$

where ϕ is the coordinate value of node and Γ_B is the boundary of the body and moving with the body. On the outside boundaries of the computational domain, Γ_U, Γ_S and Γ_D which are shown in Fig.1, coordinate ϕ is set to be 0. In this study, the behavior of the oscillating body is expressed by the relocation of nodes. Therefore, the total number of nodes and elements used by the flow analysis to solve the state equation does not change.

6.3 Algorithm

The following algorithm of the weighted gradient method is employed for the computation of the optimal shape in this study.

1. Select initial surface coordinates $X_i^{(0)}$ in Ω.
2. Solve $u_i^{(0)}$, $p^{(0)}$, $y^{(0)}$ by eqs.(9) - (16), (18) and (20) in Ω.
3. Solve $u_i^{*(0)}$, $p^{*(0)}$ by eqs.(28) - (34) in Ω.
4. Compute $X_i^{(l)}$ by eq.(48)
5. Solve $u_i^{(l)}$, $p^{(l)}$, $y^{(l)}$ by eqs.(9) - (16), (18) and (20) in Ω.
6. If $|X_i^{(l+1)} - X_i^{(l)}| < \varepsilon$ Then stop
   Else solve $u_i^{*(l)}$, $p^{*(l)}$ by eqs.(28) - (34) in Ω,
   set to $l = l + 1$, go to 4

The weighting diagonal matrix W applied to this numerical study is set as the displacement of the body does not surpass the maximum displacement of each nodes, which is 0.02 because the rapid movement of the target body destroys the finite element mesh and does not bring sure optimal shape.

6.4 Gradient computation

The gradient used for a renewal of shape is computed by the adjoint variable and the derivative of spatial direction of velocity as shown in eq.(38). Because the velocity on the body surface is zero considering the boundary condition, the gradient on the surface of the body is unable to be computed. Therefore, the linear interpolation is applied to compute $u_{j,i}$ in eq.(38) in adjacent elements around the body boundary, and the gradient is obtained as,

$$u_{j,i} = \frac{\partial u_j}{\partial X_i} = \Phi_{1,i} u_{j1} + \Phi_{2,i} u_{j2} + \Phi_{3,i} u_{j3} \tag{50}$$

where u_{j1}, u_{j2}, u_{j3} are nodal values of each element. The nodal value used for the renewal of the shape is obtained by averaging the values for the adjacent elements.

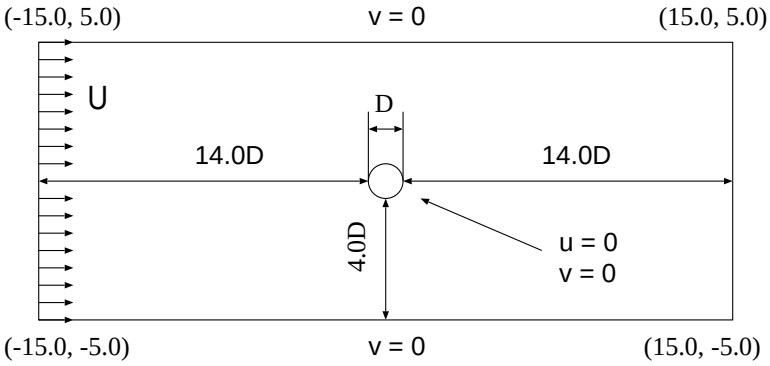

Fig.5 Computational domain and boundary condition

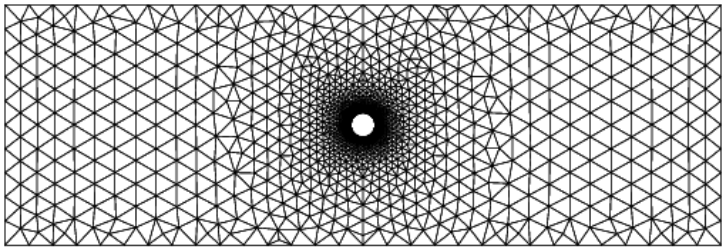

Fig.6 Finite element mesh

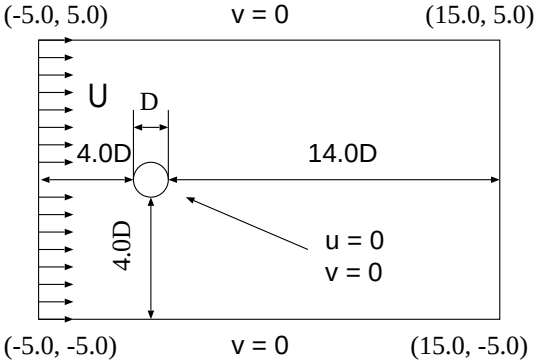

Fig.7 Computational domain and boundary condition

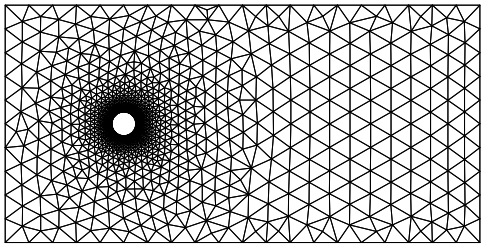

Fig.8 Finite element mesh

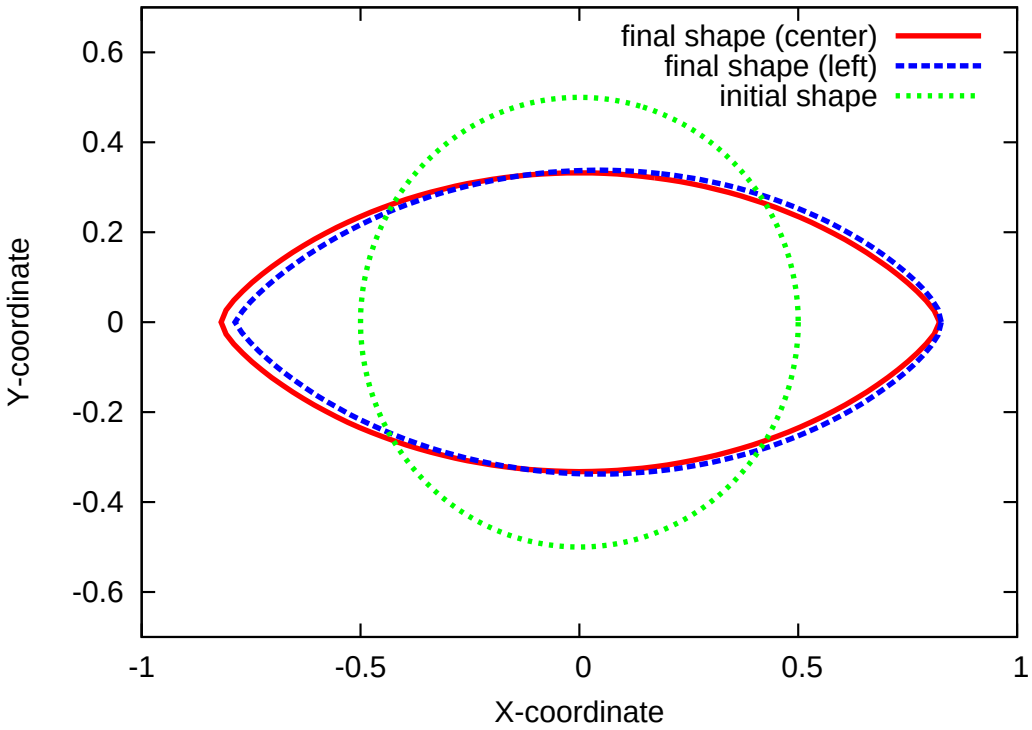

Fig.9 Comparative diagram of body coordinates

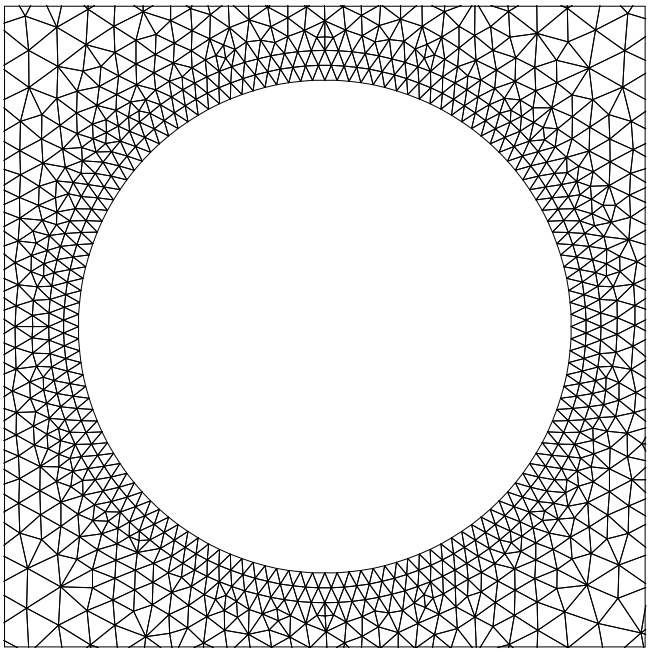

Fig.10 Magnified figure of initial shape

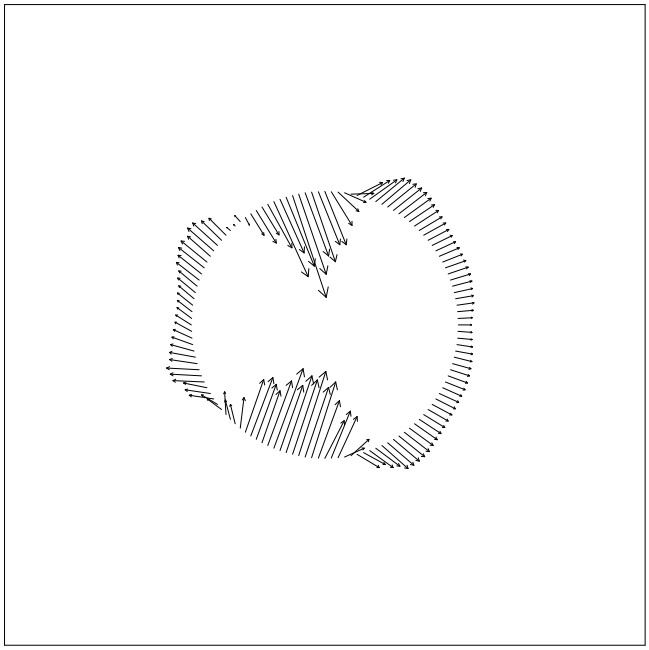

Fig.11 Gradient computed by irregular mesh around the body

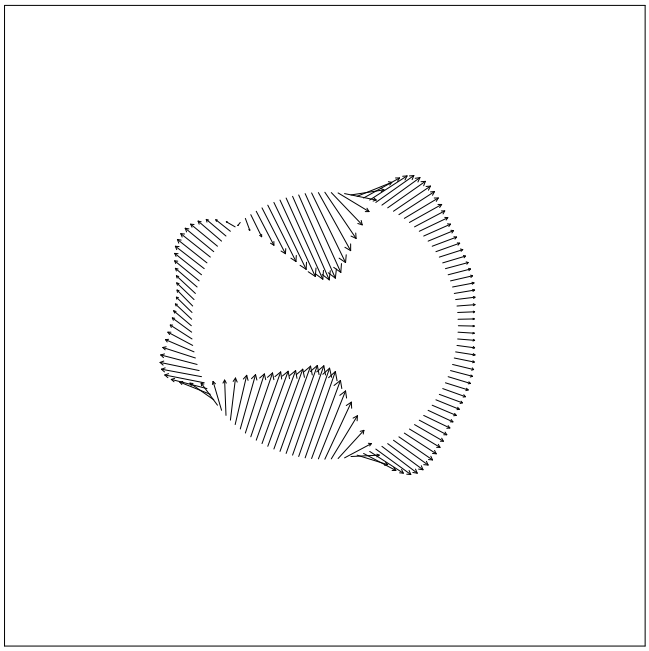

Fig.12 Gradient computed by regular mesh around the body

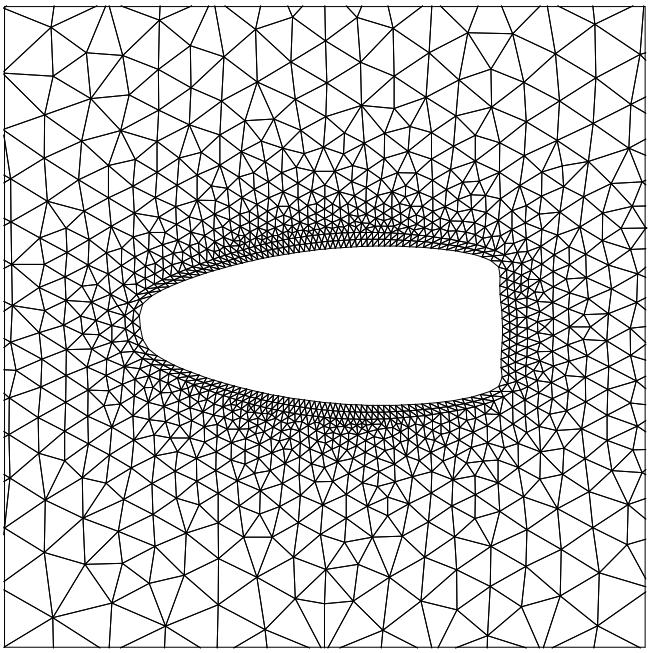

Fig.13 Intermediate shape computed after 118 iteration cycle

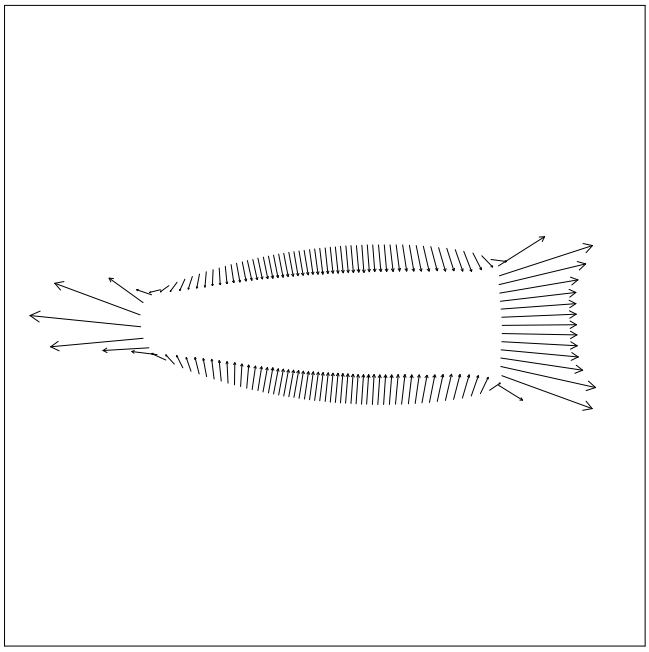

Fig.14 Gradient vector before shape of 118 iteration cycle

7 NUMERICAL RESULTS

The final shape of the body is determined under the condition that the discrepancy between the performance functions of two iteration cycles is smaller than the admissible error, 1.0×10^{-5}. After 522 iteration cycles, the final shape has been obtained. The variation of the performance function versus iteration cycle is shown in Fig.13, in which both oscillating and non-oscillating cases are described. The more stable computation is seen at the non-oscillating case. Both functions are monotonously decreasing. After 400 iteration cycles and later, almost the same performance functions have been computed.

Generally, it is known that the optimum shape of a body in the fluid flow is a streamline shape. Looking at Fig.14, the rear part of the body is thicker than the front part. This shape is different from the so called streamline form, of which a drag force affected to the body becomes small value. To reduce a lift force, it is known that a body shape is smooth and symmetrical shape with respect to the horizontal axis. At the moderate Reynolds number flow such as $Re = 250$, the optimum shape of the body located in the flow seems that the rear part of the body is thicker than the front part. The form obtained is quite similar to that of the winner of the man powered airplane race.

The gradient vector after 522 iteration cycle, which is one step before the final shape, is shown in Fig.16. The initial shape, the shape after 118 iteration cycle, 242 iteration cycle and the final shape are plotted in Fig.16. The shape of the body is going to be flat and the rear part of the body is going to be thinner according to the iteration cycle. Taking the gradient in Fig.17 into consideration, there is a possibility that the rear part is more thinner than the shape shown in Fig.16.

The time variation of the drag force comparing between initial and final shapes of the body is represented in Fig.19 and of the lift force is in Fig.20, respectively. The time variation of y displacement is shown in Fig.21. In Figs.19 - 21, the dashed line means numerical results of the initial shape and continuous line is those of the final shape, respectively. The peak values of the drag and lift forces at the final stage are reduced by 66.2 % and 92.8 %, respectively, comparing with those at the initial stage. The peak value of y displacement is also reduced by 84.8 %. The pressure distribution in the computational domain comparing between initial and final shapes of the body at non-dimensional time $T = 100$ is illustrated in Figs.22 and 23, respectively. From these figures, the pressure distribution of the final shape is completely smoothed and more scacelly vortices are found than of the initial shape. Considering those results in Figs.19 - 23, the final shape in Fig.16 can be at least close to the optimum shape of the oscillating body located in the flow of $Re = 250$.

The comparison of the final shapes of oscillating and non-oscillating bodies are represented in Fig.24. The shape of the minimum lift force is the symmetric form with respect to the horizontal axis. In the present computation, the effect of the lift force of the oscillating body is more significant than that of the non-oscillating body. Thus, the shape close to symmetric with respect to horizontal axis is obtained in case of the oscillating body.

The time variations of the drag and lift forces of the final shape of the oscillating and non-oscillating bodies are compared in Figs.25 and 26. The difference of the peak values of the drag force is 3.6 % and of the lift force is 102.8 %, respectively. Looking over the above mentioned numerical results, the difference between the oscillating and non-oscillating bodies is significant for the body located in the flow of Reynolds number $Re = 250$.

8 CONCLUSION

In this paper, the shape optimization of a body located in the transient incompressible Navier-Stokes flow has been present based on the Arbitrary Lagrangian Eulerian method. The adjoint equation and the gradient with respect to the body boundary coordinate are derived by the variation of the extended performance function, which is used for the renewal of the shape. The final shape is obtained under the condition that the performance function becomes small enough. The final shape is different from the so called streamline configuration. The drag and lift forces of the final shape of the body are drastically reduced comparing with that of the cylinder which is taken as the initial shape. The effect of the oscillation on the shape of body is so significant that the different configuration from the non-oscillating body is obtained.

The present method can be easily extended to the high Reynolds number flow. However, the definition of the optimum shape should be modified and the solution procedure should be altered. Three dimensional analysis is also adaptable but it depends on high performance computers.

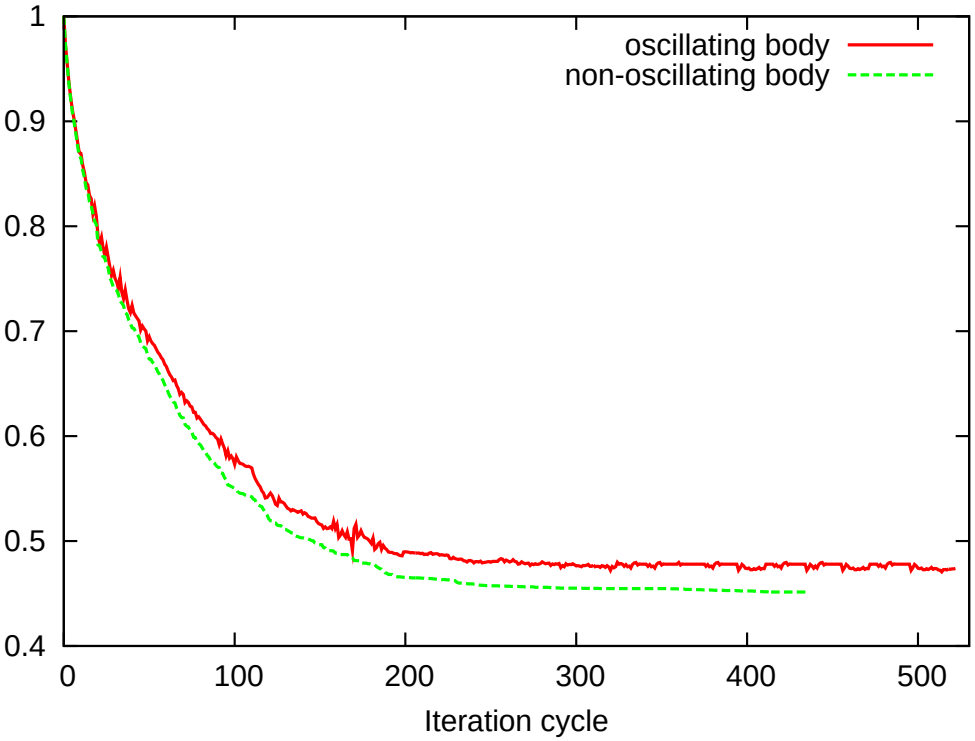

Fig.15 Variation of the performance function

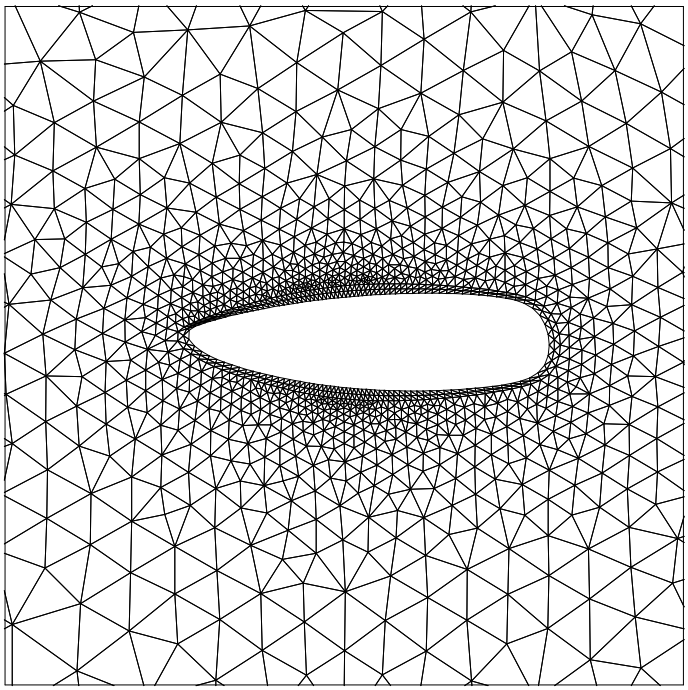

Fig.16 Final shape computed after 523 iteration cycle

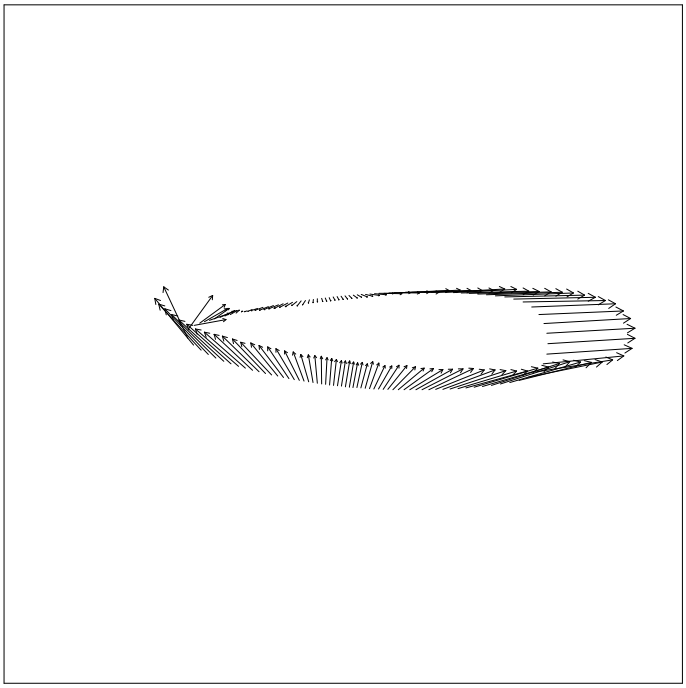

Fig.17 Gradient vector before final shape

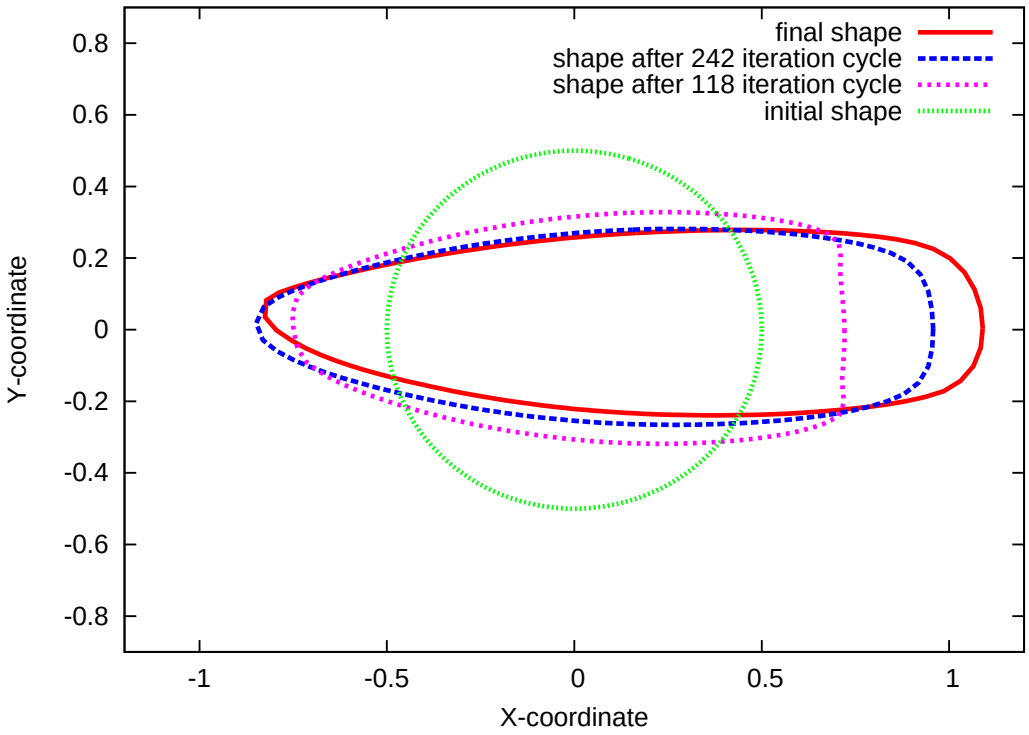

Fig.18 Comparative diagram of body coordinates

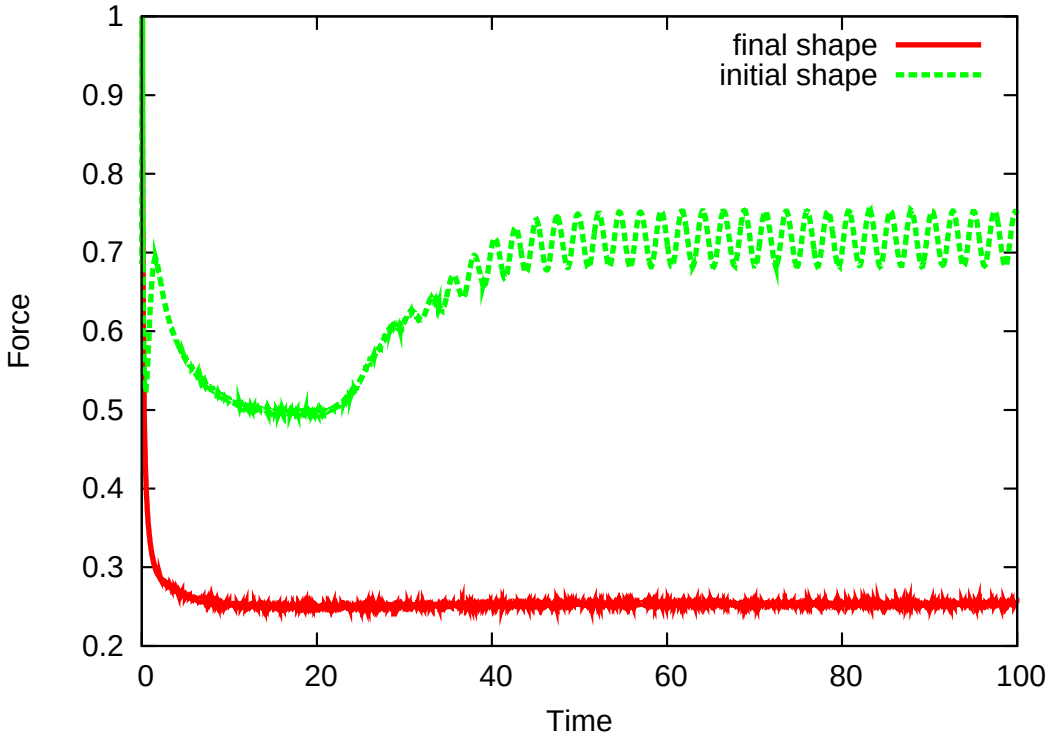

Fig.19 Time variation of drag force

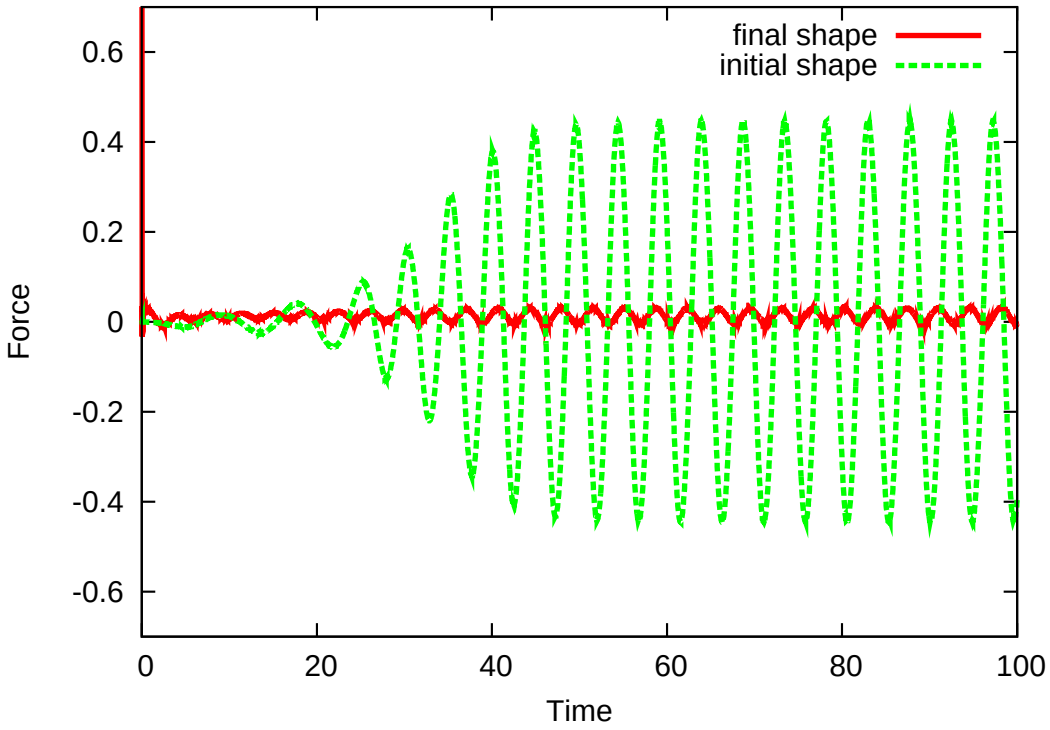

Fig.20 Time variation of lift force

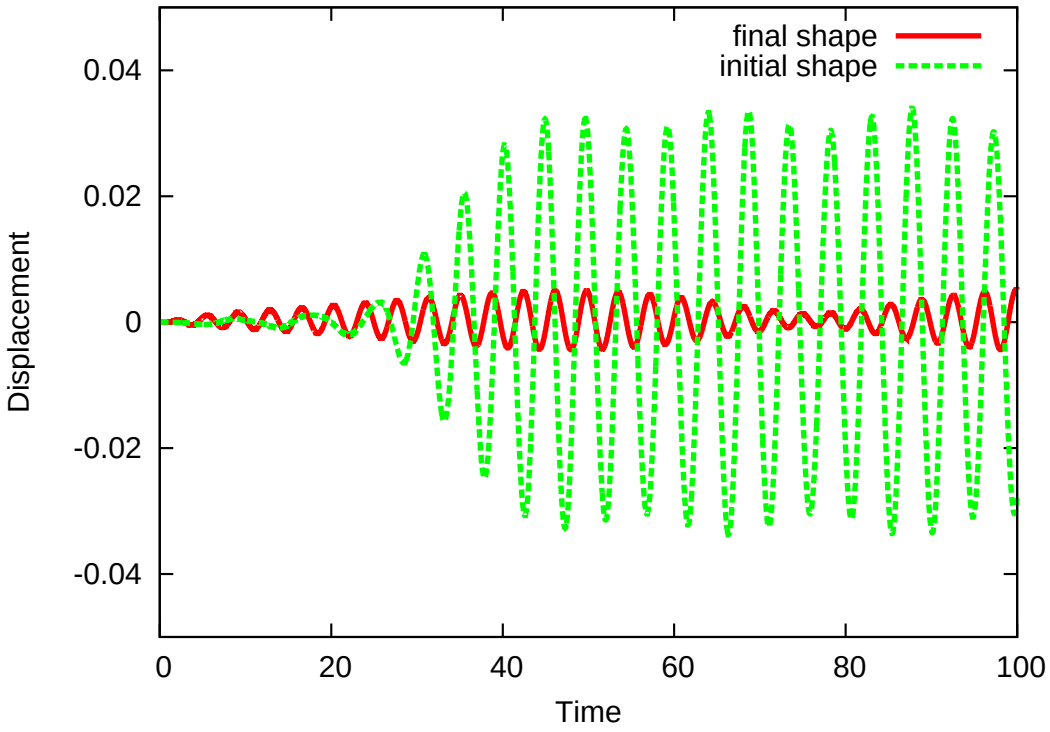

Fig.21 Time variation of displacement of y direction

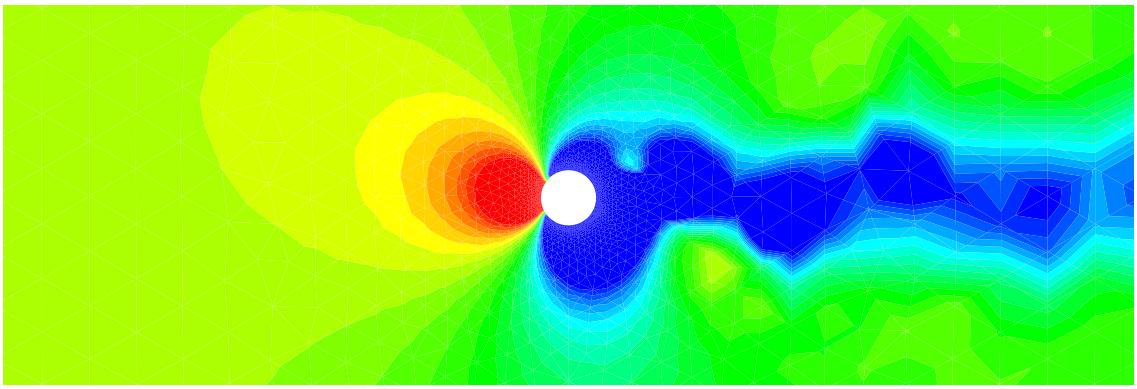

Fig.22 : Pressure distribution of the initial shape (T = 100)

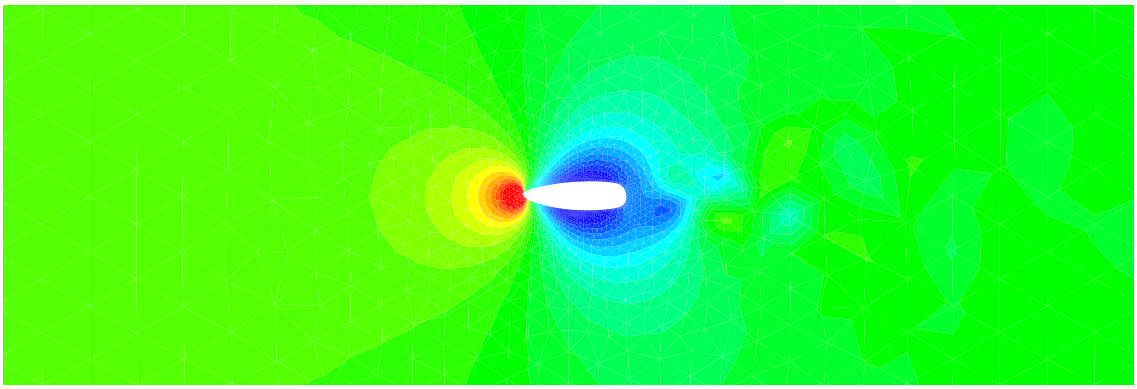

Fig.23 : Pressure distribution of the final shape (T = 100)

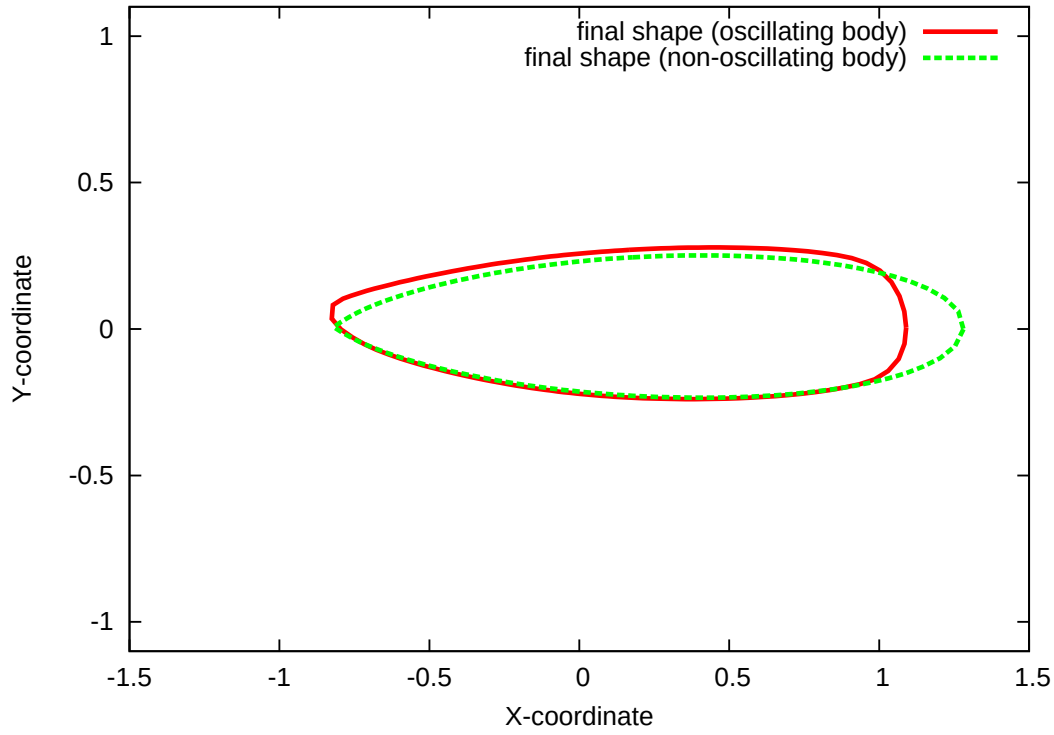

Fig.24 Comparative diagram of body coordinates

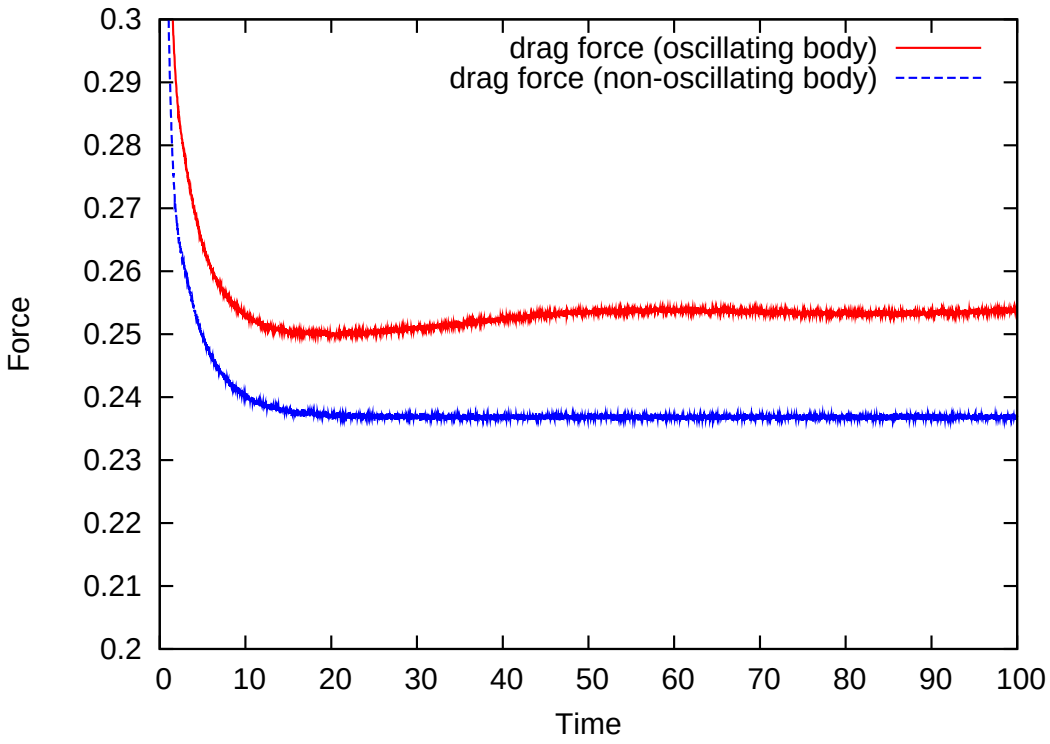

Fig.25 Time variation of drag force

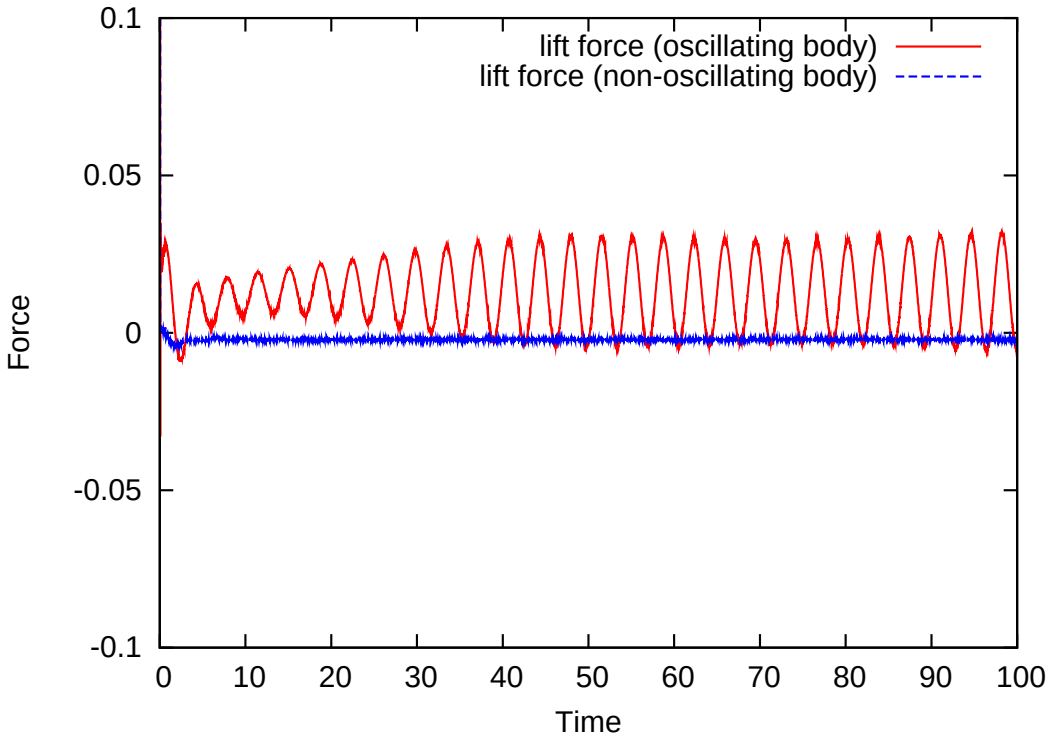

Fig.26 Time variation of lift force

References

[1] O.Pironneau : *On Optimum Profiles in Stokes Flow*. J. Fluid Mech, Vol. 59, PART 1, 1973.

[2] O.Pironneau : *On Optimum Shape Design in Fluid Mechanics*. J. Fluid Mech, Vol. 64, PART 1, 1973.

[3] B. He, O. Ghattas and J. F. Antaki : *Computational Strategies for Shape Optimization of Time-Dependent Navier-Stokes Flows*. Technical Report CMU-CML-97-102, 1997.

[4] H.Okumura and M.Kawahara : *Shape optimization of body located in incompressible Navier-Stokes flow based on optimal control theory*. CMES, Vol. 1, No.2, pp.71-77. 2000.

[5] B. Mohamadi and O. Pironneau : *Applied Shape Optimization for Fluids*. Oxford University Press, 2001.

[6] K. Leoviriyakit and A. Jameson : *Aerodynamic Shape Optimization of Wings Including Platform Variations* 44th Aero/Astro Industrial Affiliates Meeting, Stanford, April 29-30, 2003.

[7] Y.Ogawa and M.Kawahara : *Shape optimization of a body located in incompressible viscous flow based on optimal control theory*. Int. J. Comp. Fluid Dyn., Vol. 17, No.4, pp.243-251, 2003.

[8] A.Jameson : *Aerodynamic shape optimization using the adjoint method*. Lecture at the Von Karman Institute, Brussele, 2003.

[9] H.Yagi and M.Kawahara : *Shape optimization of a body located in low Reynolds number flow*. Int. J. Numer. Meth. Fluids 2005; **48**:819-833.

[10] H.Yagi and M.Kawahara : *Numerical Optimal Shape Determination of A Body Located in Incompressible Viscous Fluid Flow*. Comp. Meth. Appl. Mech. Eng., submitted.

[11] E. Katamine, H. Azegami, T. Tsubata and S. Itoh : *Solution to Shape Optimization Problems of Viscous Flow Fields*. Int. J. Comp. Fluid Dyn., Vol. 19, No.1, pp.45-51, 2005.

[12] T.J.R. Hughes, L.P.Franca and M.Balestra, *A new finite element formulation for computational fluid dynamics: V. Circumventing the Babuska-Brezzi condition: A stable Petrov-Galerkin formulation of the Stokes problem accommodating equal order interpolation*. Comp. Meth. Appl. Mech. Eng., Vol. 59, pp.85-99, 1986.

[13] J.Matsumoto, T.Umetsu and M.Kawahara, *Incompressible viscous flow analysis and adaptive finite element method using linear bubble function*. J. Appl. Mech, Vol. 2, pp.223-232, 1999. (In Japanese)

[14] E. Kuhl, S. Hulshoff and R. de Borst : *An arbitrary Lagrangian Eulerian finite-element approach for fluid-structure interaction phenomena*. Int. J. Numer. Meth. Engng 2003; **57**:117-142

[15] J. Donea, A. Huerta, J. -Ph Ponthot and A. Rodriguez-Ferran : *Arbitrary Lagrangian-Eulerian methods*. Encyclopedia of Computational Mechanics. Edited by E. Stein, R. de Borst and T. J. R. Hughes. 2004

[16] J.Matsumoto and M.kawahara : *Stable shape identification for fluid-structure interaction problem using MINI element*. J. Appl. Mech, Vol. 3, pp.263-274, 2000. (In Japanese)